PCCP

PAPER

View Article Online
View Journal | View Issue

Cite this: *Phys. Chem. Chem. Phys.*, 2023, **25**, 26613

Towards nanotube-based sensors for discrimination of drug molecules

Laith A. Algharagholy,[a] Víctor M. García-Suárez,*[b] Ohood Abdullah Albeydani[c] and Jehan Alqahtani[d]

The proper detection of drug molecules is key for applications that have an impact in several fields, ranging from medical treatments to industrial applications. In case of illegal drugs, their correct and fast detection has important implications that affect different parts of society such as security or public health. Here we present a method based on nanoscale sensors made of carbon nanotubes modified with dopants that can detect three types of drug molecules: mephedrone, methamphetamine and heroin. We show that each molecule produces a distinctive feature in the density of states that can be used to detect it and distinguish it from other types of molecules. In particular, we show that for semiconducting nanotubes the inclusion of molecules reduces the gap around the Fermi energy and produces peaks in the density of states below the Fermi energy at positions that are different for each molecule. These results prove that it is possible to design nanoscale sensors based on carbon nanotubes tailored with dopants, in such a way that they might be able to discriminate between different types of compounds and, especially, drug molecules whose proper recognition has important consequences in different fields.

Received 4th August 2023,
Accepted 20th September 2023

DOI: 10.1039/d3cp03726f

rsc.li/pccp

Introduction

Recently, illicit drug abuse has increased dramatically, and the death rate associated with its use is becoming extremely high.[1–3] To fight against the abuse of these substances, it is essential to detect different molecules. The ability to detect a wide range of illicit drugs, such as heroin, cocaine, methamphetamine and mephedrone, is, therefore, a significant challenge whose overcoming will bring great benefits to society.[4,5] The successful detection of such drugs has become a crucial priority to reduce threats and risks to public health,[6–10] which cause serious damage, such as respiratory, cardiac, renal damage and also mental health problems such as violence, depression, anxiety and hallucinations.[11,12] In order to design sensitive, fast, portable, and low-cost sensing nanodevices, it is necessary to develop new nanomaterials and device concepts, and devise new plans and strategies to control, manage, and develop precise sensor chips. Various techniques have been proposed for the detection of illicit drugs, such as mass spectrometry,[3,13,14] nuclear magnetic resonance,[15,16] X-ray powder diffraction[17] and liquid chromatography of high resolution.[18] Electrochemical or electrical methods are also promising methods and have recently grown remarkably.[19–21] Device miniaturization, on the other hand, can provide nanoscale electrical transduction capabilities,[22] which, compared to traditional techniques, leads to significant cost reductions and low power requirements. Finally, label-free techniques to detect small molecules are also desirable targets in technology, because there is no need to chemically modify or separate analytes.[23–25]

Low-dimensional materials, including heteromaterials such as nanotubes and graphene, have been intensively examined for single-molecule screening[23,24,26–35] and show promising responses, making these materials good candidates for detection applications. The synthesis of carbon nanotubes (CNTs) with various dopants has also been reported using different experimental techniques, for example, CNTs doped with boron[36,37] and nitrogen.[38] Junction fabrication is also an important step that must be completed to design suitable sensors. Despite many obstacles, involving the precise preparation of carbon nitride/boron heterojunctions, successful experimental attempts have been carried out using different methods.[39–46] These heterojunctions are energetically stable[24,39,47–49] and have electronic properties that can be modified by changing the width of the boron nitride strips in the heteronanotube.[23,50]

Results

In this work, we aim at sensing three types of illicit drug molecules, namely mephedrone (MEP, with chemical formula

[a] *Department of Physics, College of Science, University of Sumer, Al-Rifaee, 64005, Thi-Qar, Iraq*
[b] *Departamento de Física, Universidad de Oviedo & CINN, Oviedo, 33007, Spain. E-mail: vm.garcia@cinn.es, garciavictor@uniovi.es*
[c] *Department of Physics, Faculty Science, Taibah University, Yanbu 46423, Saudi Arabia*
[d] *Department of Physics, Faculty Science, King Khalid University, Abha 62529, Saudi Arabia*

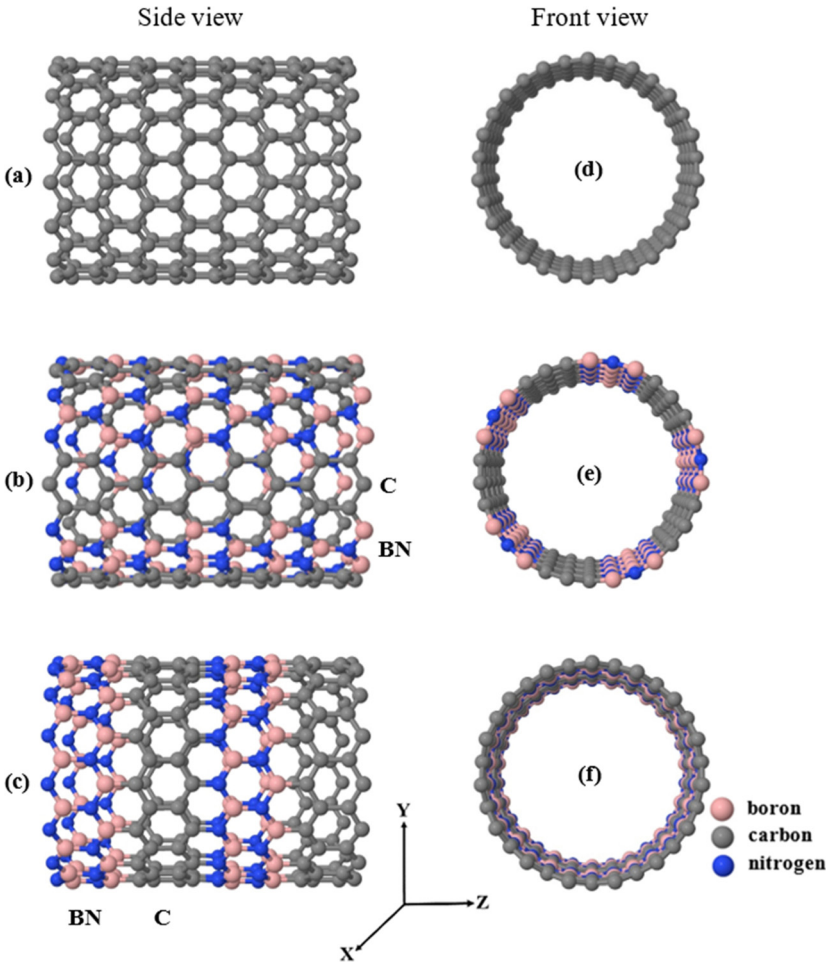

Fig. 1 Side view (a)–(c) and front view (d)–(f) of the relaxed ideal ZCNT, *h*-hZNT, and *v*-hZNT nanotubes respectively. BN and C indicate boron nitride and carbon strips in the hetero-nanotubes shown in subfigures (b) and (c). All nanotubes are periodic in the *Z* direction and isolated in the *X* and *Y* directions.

$C_{11}H_{15}NO$), methamphetamine (MET, $C_{10}H_{15}N$), and heroin (HER, $C_{21}H_{24}NO_5$) by encapsulating them inside different types of nanotubes and calculating the subsequent modification of their electronic properties. Note that the encapsulation of molecules and other nanometric compounds inside nanotubes has been carried out for a relatively long time with different experimental techniques and in all cases the electronic structure was modified upon such encapsulation.[51–56] Currently, the MEP, MET, and HER molecules are widely abused and considered harmful substances, causing a variety of health problems, including mental illness.[57–60] Herein, we examine three different (15.0) zigzag nanotubes with different compositions for the selective detection of MEP, MET, and HER. We start with an ideal (15,0) zigzag carbon nanotube (ZCNT), shown in Fig. 1a, which behaves as metallic with an almost zero-energy gap E_g (notice, however, that due to curvature effects these nanotubes exhibit a narrow band gap[61–63]), and follow with two different striped (15,0) hetero-nanotubes composed of carbon, boron, and nitrogen atoms. Note as well that the modification of carbon nanotubes with different types of atoms, such as B and N, has also been done experimentally for a relatively long time.[38,64,65] Fig. 1b shows the first type of striped hetero-nanotube, which consists of rows of hexagonal rings of boron nitride (BN) and carbon (C) that spread along the longitudinal direction (*Z*-axis); Fig. 1c shows the second type of striped hetero-nanotube, which contains boron nitride (BN) and carbon (C) rings oriented along the transverse direction (*Y*-axis). Conveniently, we refer from now on to the striped hetero-nanotubes shown in Fig. 1(b and c) as *h*-hZNT and *v*-hZNT respectively.

We use density functional theory (DFT), as implemented in the SIESTA code (see the computational tools section for more details). After achieving the optimized ground state structures, we used the mean-field Hamiltonian obtained from SIESTA to calculate the density of states (DOS) for the bare nanotubes, shown in Fig. 1. The DOS, which represents the number of states as a function of energy (whose integration up to the Fermi level gives the number of electrons) is a quantity that is typically used to characterize the electronic properties of a material or compound. As can be seen, the DOS calculated for the *h*-hZNT and *v*-hZNT shown in Fig. 2 have a markedly different shape than the ideal ZCNT, which shows a zero

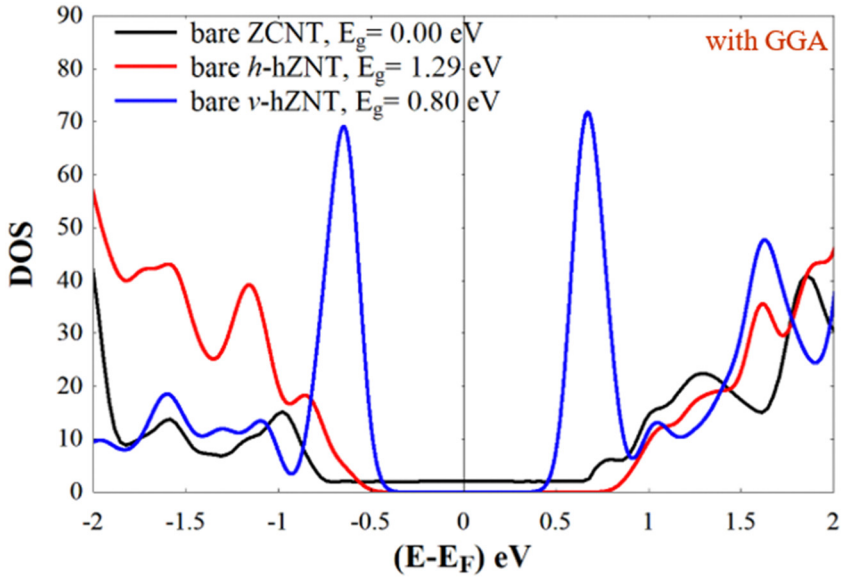

Fig. 2 Density of states (DOS) of the bare nanotubes shown in Fig. 1.

(metallic) energy gap, *i.e.* adding the BN strips strongly modifies the electronic structure, as Was expected. We find that the *h*-hZNT and *v*-hZNT have energy gaps of 1.28 eV and 0.78 eV respectively, which are close to the energy gap of silicon (1.12 eV)[66,67] and the germanium (0.74 eV)[68,69] (actually they would be slightly larger, almost double due to underestimation of the gap by DFT; notice however, that such underestimation should not modify the emergence of the molecular resonances close to the Fermi level, nor their relative position, since the resonances are associated to the molecules and usually appear within the gap. This makes these hetero-nanotubes promising semiconductor materials for a variety of electronic applications.

We first calculate the binding energy (E_B) for the relaxed molecules inside the nanotubes, to check whether it is favourable or not to encapsulate the molecules. The binding energy allows to assess the final result of the encapsulation irrespective of the path followed to make it (notice for instance that a full study of such encapsulation would require the calculation of the height and width of the potential barrier when the molecule and the nanotube approach each other -if the potential barrier were too high then it would be necessary to add additional energy to encapsulate the particular molecule- and the consideration of several details such as the structure of the opening, its composition, *etc.*) We use the following equation, which also takes into account the basis-set superposition error (BSSE) due to the fact that the Hilbert space of the susbsystems is not the same when atomic orbitals are used:[70,71]

$$E_B = E^{NT+Mol} - (E^{NT}_{G,Mol} + E^{Mol}_{G,NT}) \quad (1)$$

E^{NT+Mol} represents the total energy of the whole system, *i.e.*, the molecule encapsulated in the nanotube, $E^{Mol}_{G,NT}$ is the energy of the nanotube in the presence of the ghost states of the molecule (*i.e.* atomic orbitals without the corresponding atomic potential) and $E^{Mol}_{G,NT}$ is the energy of the molecule in the presence of the ghost states of the nanotube. Table 1 shows the resulting binding energies of MEP, MET, and HER within the nanotubes. Most of the energies are negative, which by eqn (1) implies that the formation of the combined system is exothermic and therefore can be created without additional energy. Note that ZCNT + MEP and ZCNT + MET are endothermic but become exothermic when encapsulated in the other nanotubes, *i.e.* in case of ZCNT the process of encapsulation needs additional energy, but occurs spontaneously in the other two nanotubes. This demonstrates the importance of designing and choosing suitable heteronanotubes for the formation of these systems. Also, the most stable configurations are those that involve HER, *i.e.* ZCNT + HER, with E_B equal to −1.0151 eV, *h*-hZNT + HER, with E_B equal to −1.8390 eV, and *v*-hZNT + HER, with E_B equal to −0.9723 eV). This order of stabilities is somewhat expected, because HER is the biggest molecule and interacts more strongly with the nanotube walls. Notice as well that the inclusion of BN rows (*h*-hZNT) or rings (*v*-hZNT) in the original carbon nanotube increases in general the stability (more negative binding energies). This and the previous points

Table 1 Binding energies of MEP, MET, and HER drug molecules inside the corresponding nanotubes

Nanotube + molecule	E_B (eV)	Nanotube + molecule	E_B (eV)	Nanotube + molecule	E_B (eV)
ZCNT + MEP	0.2856	*h*-hZNT + MEP	−1.4337	*v*-hZNT + MEP	−0.1764
ZCNT + MET	0.9853	*h*-hZNT + MET	−0.0941	*v*-hZNT + MET	−0.0636
ZCNT + HER	−1.0151	*h*-hZNT + HER	−1.8390	*v*-hZNT + HER	−0.9723

Table 2 Charge transfer (C_T) between the nanotubes and the drug molecules. The values are given in electrons per molecule. Negative values mean that the molecules lose charge

Nanotube + molecule	C_T	Nanotube + molecule	C_T	Nanotube + molecule	C_T
ZCNT + MEP	0.124 *e*	*h*-hZNT + MEP	0.084 *e*	*v*-hZNT + MEP	−0.150 *e*
ZCNT + MET	−0.092 *e*	*h*-hZNT + MET	0.050 *e*	*v*-hZNT + MET	−0.033 *e*
ZCNT + HER	0.110 *e*	*h*-hZNT + HER	0.101 *e*	*v*-hZNT + HER	0.107 *e*

show the importance of designing heteronanotubes with tailored properties.

We have also carried out Mulliken charge analyses of the MEP, MET, and HER drug molecules and the nanotubes to estimate the amount of charge transfer (C_T) between both subsystems, which can shed light on their electronic properties. The results are shown in Table 2. As can be seen, the larger amount of C_T occurs for the MEP molecule encapsulated inside *v*-hZNT and is equal to −0.150 *e*. The negative sign means that the charge is transferred to the nanotube from the molecule,[72] *i.e.* in ZCNT + MET, *v*-hZNT + MEP and *v*-hZNT + MET the molecule loses charge and behaves as an electron donor. In the case of HER, however, the charge transfer is always positive, which is to be expected since this molecule has more electronegative atoms (O and N) than the other two molecules. In general, the charge transfers are small and change with the type of molecule and nanotube, again indicating that the donor or acceptor behavior of these molecules can be modified with a suitable choice of heteronanotube. These charge transfers can also be seen experimentally[73] and provide another possible indicator of the presence of the molecules within the nanotubes.

In what follows, we investigate the potential of the ideal ZCNT and the *h*-hZNT and *v*-hZNT for detection of target analytes (MEP, MET, and HER molecules). First, we encapsulate MEP, MET, and HER within the nanotubes and then relax the initial supercell to achieve the final relaxed structures. Fig. 3 shows the relaxed structures of the molecules both outside and inside the ZCNT. Note also that the encapsulation of molecules within carbon nanotubes has been demonstrated experimentally.[74–78] We then calculated the DOS of the nanotubes in the presence of the analytes. Fig. 4 shows the resulting DOS for ZCNT + MEP, ZCNT + MET, and ZCNT + HER.

From Fig. 4 and comparing the DOS of the ideal ZCNT shown in Fig. 2, we can see that encapsulating MEP, MET, and HER molecules inside the ZCNT gives rise to a new feature in the DOS below the Fermi energy (E_F). Fig. 4 shows that new peaks appear due to the presence of the analytes in the DOS of ZCNT + MEP, ZCNT + MET, and ZCNT + HER. These peaks are located, as commented before, below E_F and have their maxima

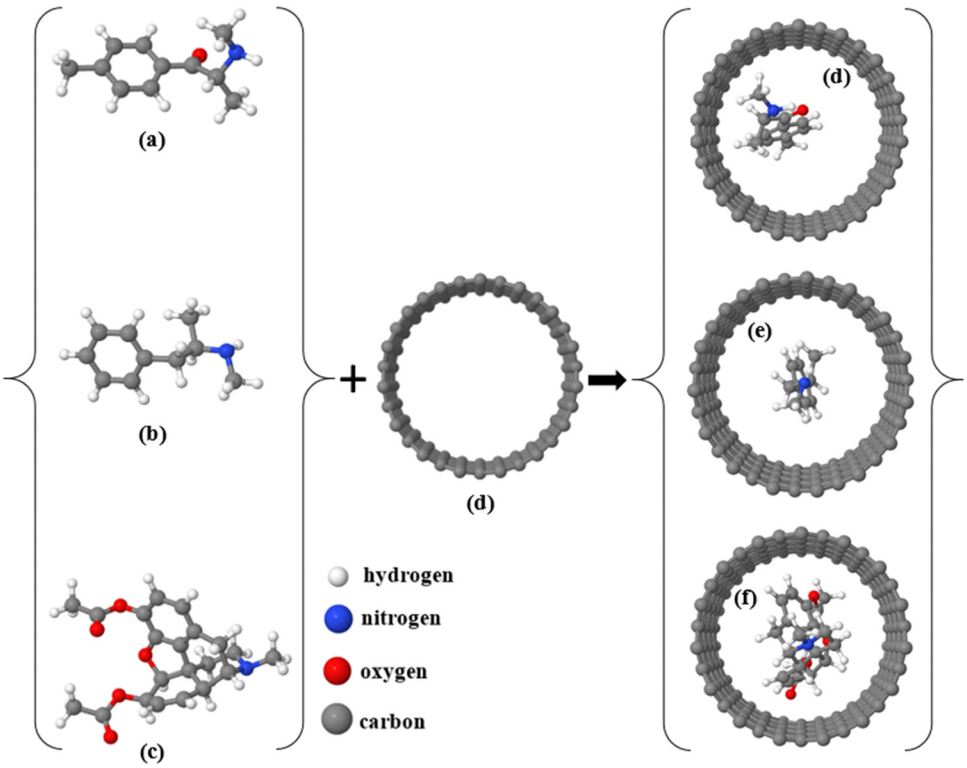

Fig. 3 (a)–(d) The targeted drug molecules MEP, MET, and HER respectively, (d) the bare ideal ZCNT, and (d)–(f) the final relaxed structures of each drug molecule encapsulated within the ideal ZCNT, *i.e.* ZCNT + MEP, ZCNT + MET, and ZCNT + HER, respectively.

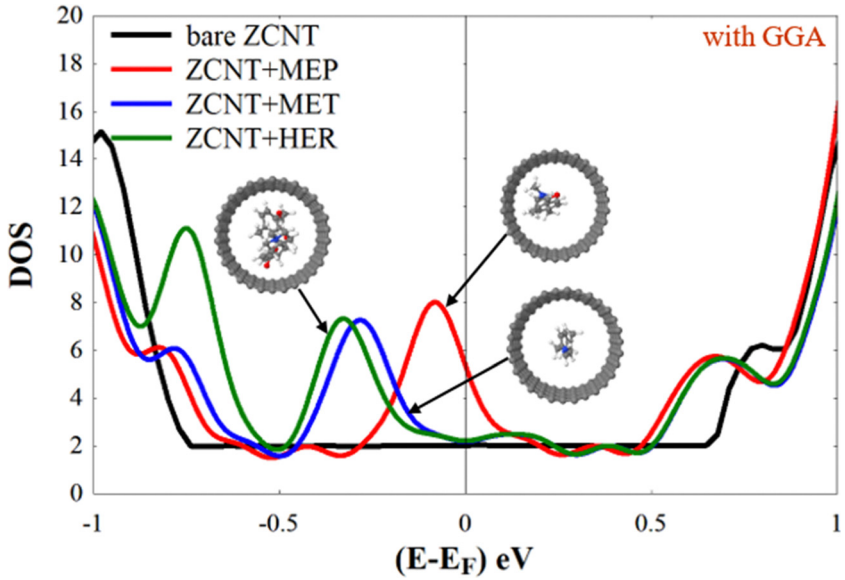

Fig. 4 Density of states (DOS) for ZCNT + MEP, ZCNT + MET, and ZCNT + HER.

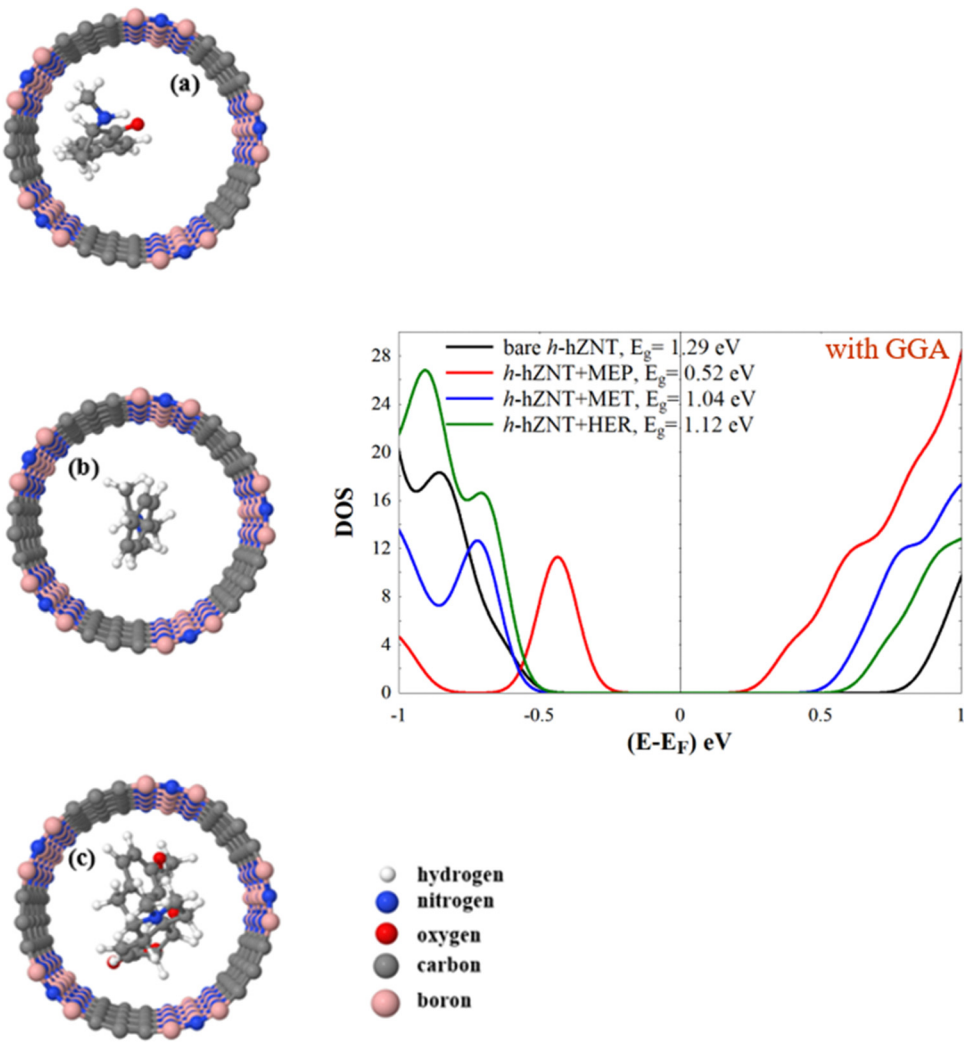

Fig. 5 (a)–(c) Relaxed *h*-hZNT + MEP, *h*-hZNT + MET, and *h*-hZNT + HER, respectively, and the corresponding densities of states (panel on the right).

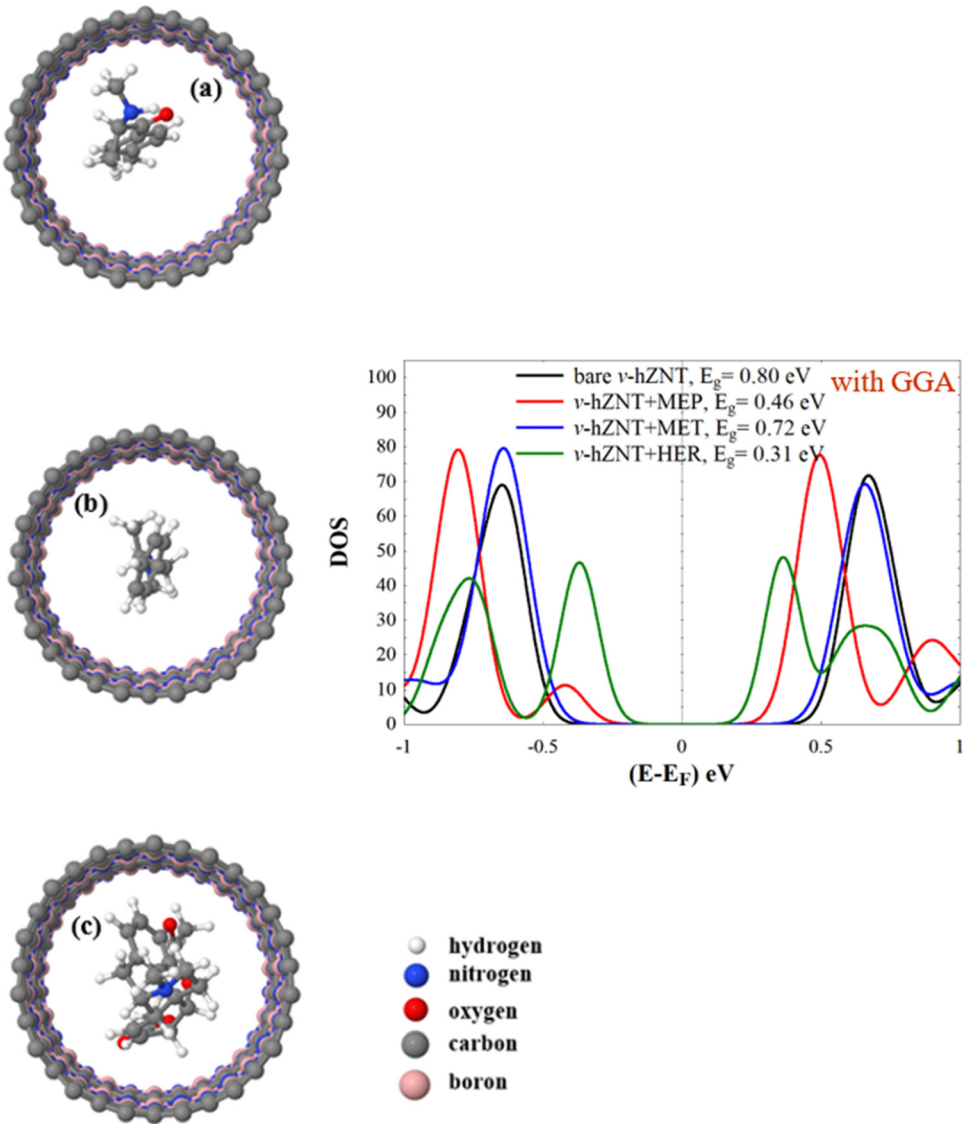

Fig. 6 (a)–(c) Relaxed *v*-hZNT + MEP, *v*-hZNT + MET, and *v*-hZNT + HER, respectively, and the corresponding density of states (panel on the right).

at −0.080 eV, −0.286 eV, and −0.330 eV respectively. These new extra features, which appear close to E_F (below it), could be measured by sampling the DOS of the combined systems in *e.g.* experiments involving the scanning tunnelling microscope, by measuring the conductance by connecting the nanotubes to proper electrodes or by easier and faster methods that would involve optical properties, such as visible range spectroscopy.[79,80] The calculation of optical properties such as fluorescence differences would also require the use of TDDFT,[81] which may lead to future avenues of research for these systems. In addition, due to their shape and position, such features can also lead to improvements of the Seebeck coefficient,[26,39,82,83] and thus can also be used for selective sensing of MEP, MET, HER by means of the Seebeck effect.

Using the same scenario shown in Fig. 3, we relax the MEP, MET, and HER molecules inside *h*-hZNT and *v*-hZNT. The final relaxed structures are shown in Fig. 5(a–c) and 6(a–c). Right subfigures in Fig. 5 and 6 also show the obtained DOS for the *h*- and *v*- relaxed hZNT + MEP, hZNT + MET, and hZNT + HER, respectively. It is clear from Fig. 5 that, compared to the DOS of *h*-hZNT in the absence of the molecules, there is a remarkable non-trivial reduction of the energy gap in the DOS for *h*-hZNT + MEP, *h*-hZNT + MET, and *h*-hZNT + HER due to the presence of the molecules. Furthermore, a new peak below E_F appears again in the resulting DOS, which is clearly different for each type of molecule. The peaks are located at −0.426 eV, −0.698 eV and −0.727 eV for *h*-hZNT + MEP, *h*-hZNT + MET and *h*-hZNT + HER, respectively. Note that for this heteronanotube the peak positions and relative order are different than for pure ZCNT. The peaks also allow to distinguish between the three molecules, although the MET and HER peaks are close together.

Similarly, for *v*-hZNT + MEP, *v*-hZNT + MET, and *v*-hZNT + HER the DOS show that the insertion of the drug molecules inside this nanotube leads again to a reduction of the energy gap, compared to the bare *v*-hZNT. The largest reduction of the

gap occurs for HER and the smallest for MET (*i.e.* the size of the gap in *v*-hZNT + MET is the most similar to that of the bare *v*-ZNT). In this case, however, only one system, *v*-hZNT + MEP, shows an additional peak below E_F. The differences between all the molecules arise, however, below or above the energy gap (different amplitudes and positions of the corresponding peaks). Such differences should also be measurable by sampling the DOS of these systems. Therefore, we can conclude that by measuring the size of the space or the features inside, above, or below it, it is possible to clearly detect the presence of each type of molecule.

Discussion

From the results it is clear that the introduction of the drug molecules inside the nanotubes leads to non-trivial changes that should allow an adequate detection of said substances. The doping of the nanotubes with impurities of B and N is also an important factor that helps to increase the detection properties of these systems. The most notable modification of the electronic structure is the appearance of resonances around the Fermi level that can be easily seen in DOS. These resonances come from the presence of molecular states close to the Fermi level, which are obviously different for each of them due to their different composition and structure. The position of such resonances also depends on various factors that determine their exact position, such as the charge transfer between the nanotube and the molecule and the interaction of the latter with the nanotube wall, factors that are always present in the encapsulation of atoms or molecules inside nanotubes.[84] The first factor changes the position of the levels of both systems, while the second leads to additional changes in the states due to slight modifications of the structures (changes in the angles and distances between atoms; this is verified by comparing the coordinates before and after the encapsulation).

On the other hand, the inclusion of dopant impurities with certain periodicities inside the nanotubes causes strong modifications in the electronic structure of the nanotubes, which makes them semiconductors. This is also to be expected, since BN hexagonal structures are insulators and their inclusion in carbon nanotubes breaks the structural continuity between the carbon lattice and opens a bandgap.[38,64,65] Such a change (from metallic to semiconductor) also increases the detection properties of the systems, as also expected, since the effect of the resonances of the molecules becomes clearer if the nanotube does not have states around the Fermi level that can mask the effect of such resonances or hybridize with them and change their current position. Taken together, the design presented in this article (molecules encapsulated in modified nanotubes) proves that it might be possible to detect different types of compounds and possibly discriminate between them (since in some cases the resonances are closed to each other and might be difficult to assign to a particular molecule) by encapsulating them in carbon nanotubes.

Conclusions

Using first principles, we have calculated the electronic properties of three types of drug molecules, mephedrone, methamphetamine and heroin, encapsulated in three types of nanotubes, two of which are built by replacing carbon rows or rings with hBN structures. We first show that by using different types of BN strips it is possible to tailor the electronic properties of nanotubes and convert them into semiconductor systems with gaps similar to those of typical semiconductors.

By encapsulating the molecules in the nanotubes, we found that the combined systems were generally exothermic, implying that these compounds can be formed without additional energy. It is important to note that the only two cases that were endothermic, ZCNT + MEP and ZCNT + MET, become exothermic when pure ZCNT is replaced by heteronanotubes. We have also calculated the charge transfer and found that it depends on the type of molecule and nanotube, but in general, the more electronegative the molecule (HER), the greater the charge transfer to it from the nanotube, leading to negatively charged nanotube walls.

By analyzing the density of states of the combined systems, we find that the molecules might produce a distinctive feature below the Fermi energy, especially for the cases of ZCNT and *h*-hZNT. For the *v*-hZNT, however, no distinctive peaks are observed for MET and HER and the differences are twofold: a reduction in the energy gap and changes in features above and below it. These DOS modifications depend on the type of molecule and nanotube and prove two things: first, that it is possible in general to detect these three molecules using nanotubes; second, that the type of nanotube is also important to detect the molecules, since it leads to different characteristics that can be used for said detection.

Computational tools

To obtain the final ground state, the relaxed geometry and the mean-field Hamiltonian (MFH), we used the SIESTA[85] implementation of density functional theory (DFT). We employed the local density approximation (LDA)[86] with the Ceperley–Alder (CA) exchange correlation functional and also, to further verify the results, the generalized gradient approximation (GGA),[87] which is the one we took to show the results. We note that the LDA and GGA results agree rather well, with some minor differences in the position of the peaks, while their relative position is kept, which shows the feasibility of these calculations to make predictions. We have also used a double-ζ polarized (DZP) basis sets of pseudo atomic orbitals, which is enough to describe carbon-based systems and light elements,[88] and a real-space grid defined with a plane wave cut-off energy of 300 Ry. The initial structures were relaxed until the total forces of all the atoms were smaller than 0.01 eV $Å^{-1}$. For all the DOS calculations, we sampled the Brillouin zone with a *k*-point grid of $1 \times 1 \times 30$. The DOS was artificially broadened with a factor of 0.1 eV, which is small enough to clearly distinguish the resonances. To assure that there was no interaction between

the analytes encapsulated inside the nanotubes and the periodic images along the nanotube axis, we ensured that the distance between the targeted molecules was enough to avoid such interactions. For instance, in the case of ZCNT + HER, *h*-hZNT + HER, and *v*-hZNT + HER, the distances were 5.6 Å, 5.4 Å, 5.3 Å, respectively, while for the other molecules they were larger than 6.8 Å.

Author contributions

Laith A. Algharagholy, V. M. García-Suárez, Ohood Abdullah Albeydani, and Jehan Alqahtani were involved in interpreting the results, writing, and commenting the manuscript.

Conflicts of interest

The authors declare no conflict of interest.

Acknowledgements

Laith A. Algharagholy acknowledges the Iraqi Ministry of Higher Education and Scientific Research and University of Sumer for the support. V. M. García-Suárez acknowledges funding from the project PGC2018-094783 (MCIU/AEI/FEDER, EU). Ohood Abdullah Albeydani and Jehan Alqahtani acknowledge Taibah University and King Khalid University, Saudi Arabia, for the support.

References

1 N. Wilson, *et al.*, Drug and opioid-involved overdose deaths—United States, 2017–2018, *Morb. Mortal. Wkly. Rep.*, 2020, **69**(11), 290.
2 D. Lewer, *et al.*, Causes of death among people who used illicit opioids in England, 2001–18: a matched cohort study, *Lancet*, 2022, **7**(2), e126–e135.
3 S. Azimi and A. Docoslis, Recent advances in the use of surface-enhanced Raman scattering for illicit drug detection, *Sensors*, 2022, **22**(10), 3877.
4 K. Liu, *et al.*, Unambiguous Discrimination and Detection of Controlled Chemical Vapors by a Film-Based Fluorescent Sensor Array, *Adv. Mater. Technol.*, 2019, **4**(7), 1800644.
5 R. Boroujerdi and R. Paul, Graphene-Based Electrochemical Sensors for Psychoactive Drugs, *Nanomaterials*, 2022, **12**(13), 2250.
6 P. Esseiva, *et al.*, A methodology for illicit heroin seizures comparison in a drug intelligence perspective using large databases, *Forensic Sci. Int.*, 2003, **132**(2), 139–152.
7 L. Dujourdy, *et al.*, Evaluation of links in heroin seizures, *Forensic Sci. Int.*, 2003, **131**(2–3), 171–183.
8 S. Gandhi, *et al.*, Recent advances in immunosensor for narcotic drug detection, *BioImpacts*, 2015, **5**(4), 207.
9 A. Florea, *et al.*, Electrochemical sensing of cocaine in real samples based on electrodeposited biomimetic affinity ligands, *Analyst*, 2019, **144**(15), 4639–4646.
10 A. Quaranta, *et al.*, Illegal drugs and periodontal conditions, *Periodontology*, 2022, **90**(1), 62–87.
11 G. Daziani, *et al.*, Synthetic Cathinones and Neurotoxicity Risks: A Systematic Review, *Int. J. Mol. Sci.*, 2023, **24**(7), 6230.
12 T. T. Khame and M. Mhaka-Mutepfa, Impact of Illicit Substances on Health, *Substance Use and Misuse in sub-Saharan Africa: Trends, Intervention, and Policy*, 2021, pp. 95–109.
13 C. Yuan, D. Chen and S. Wang, Drug confirmation by mass spectrometry: Identification criteria and complicating factors, *Clin. Chim. Acta*, 2015, **438**, 119–125.
14 F. Hernández, *et al.*, Mass spectrometric strategies for the investigation of biomarkers of illicit drug use in wastewater, *Mass Spectrom. Rev.*, 2018, **37**(3), 258–280.
15 G. Assemat, *et al.*, Benchtop low-field 1H Nuclear Magnetic Resonance for detecting falsified medicines, *Talanta*, 2019, **196**, 163–173.
16 N. Burns, *et al.*, The identification of synthetic cannabinoids surface coated on herbal substrates using solid-state nuclear magnetic resonance spectroscopy, *Anal. Chim. Acta*, 2020, **1104**, 105–109.
17 Y.-D. Dong and B. J. Boyd, Applications of X-ray scattering in pharmaceutical science, *Int. J. Pharm.*, 2011, **417**(1–2), 101–111.
18 C. Hubert, *et al.*, Validation of an ultra-high-performance liquid chromatography-tandem mass spectrometry method to quantify illicit drug and pharmaceutical residues in wastewater using accuracy profile approach, *J. Chromatogr. A*, 2017, **1500**, 136–144.
19 L. Su, Overview on the sensors for direct electrochemical detection of illicit drugs in sports, *Int. J. Electrochem. Sci.*, 2022, **17**(221260), 2.
20 S. Bilge, *et al.*, Recent advances in electrochemical sensing of cocaine: A review, *TrAC, Trends Anal. Chem.*, 2022, 116768.
21 R. Moradi, *et al.*, Nanoarchitectonics for Abused-Drug Biosensors, *Small*, 2022, **18**(10), 2104847.
22 H. Sadeghi, *et al.*, Graphene sculpturene nanopores for DNA nucleobase sensing, *J. Phys. Chem. B*, 2014, **118**(24), 6908–6914.
23 L. Algharagholy, *et al.*, Sensing single molecules with carbon–boron-nitride nanotubes, *J. Mater. Chem. C*, 2015, **3**(39), 10273–10276.
24 L. A. Algharagholy, H. Sadeghi and A. A. Al-Backri, Selective sensing of 2, 4, 6-trinitrotoluene and triacetone triperoxide using carbon/boron nitride heteronanotubes, *Mater. Today Commun.*, 2021, **28**, 102739.
25 B. Lin, *et al.*, A label-free optical technique for detecting small molecule interactions, *Biosens. Bioelectron.*, 2002, **17**(9), 827–834.
26 L. A. Algharagholy, *et al.*, Discriminating sensing of explosive molecules using graphene–boron nitride–graphene heteronanosheets, *RSC Adv.*, 2022, **12**(54), 35151–35157.
27 H. Rahman, M. R. Hossain and T. Ferdous, The recent advancement of low-dimensional nanostructured materials for drug delivery and drug sensing application: A brief review, *J. Mol. Liq.*, 2020, **320**, 114427.
28 A.-M. Dragan, *et al.*, Electrochemical fingerprints of illicit drugs on graphene and multi-walled carbon nanotubes, *Front. Chem.*, 2021, **9**, 641147.

29 Y. Zhang, *et al.*, Sensing methamphetamine with chemiresistive sensors based on polythiophene-blended single-walled carbon nanotubes, *Sens. Actuators, B*, 2018, **255**, 1814–1818.
30 A. Navaee, A. Salimi and H. Teymourian, Graphene nanosheets modified glassy carbon electrode for simultaneous detection of heroine, morphine and noscapine, *Biosens. Bioelectron.*, 2012, **31**(1), 205–211.
31 D. Krepel and O. Hod, Selectivity of a graphene nanoribbon-based trinitrotoluene detector: a computational assessment, *J. Phys. Chem. C*, 2017, **121**(39), 21546–21552.
32 F. Patolsky, G. Zheng and C. M. Lieber, Fabrication of silicon nanowire devices for ultrasensitive, label-free, real-time detection of biological and chemical species, *Nat. Protoc.*, 2006, **1**(4), 1711–1724.
33 S. S. Varghese, *et al.*, Recent advances in graphene based gas sensors, *Sens. Actuators, B*, 2015, **218**, 160–183.
34 J. Mawwa, *et al.*, In-plane graphene/boron nitride heterostructures and their potential application as toxic gas sensors, *RSC Adv.*, 2021, **11**(52), 32810–32823.
35 C. Wei, *et al.*, Pt-decorated BC2N graphene-like nanosheet as a promising sensor for benzoylethanamine drug, *Thin Solid Films*, 2020, **712**, 138313.
36 K. McGuire, *et al.*, Synthesis and Raman characterization of boron-doped single-walled carbon nanotubes, *Carbon*, 2005, **43**(2), 219–227.
37 F. Monteiro, *et al.*, Production and characterization of boron-doped single wall carbon nanotubes, *J. Phys. Chem. C*, 2012, **116**(5), 3281–3285.
38 P. Ayala, *et al.*, The doping of carbon nanotubes with nitrogen and their potential applications, *Carbon*, 2010, **48**(3), 575–586.
39 L. A. Algharagholy and V. M. García-Suárez, Defect-Induced Transport Enhancement in Carbon–Boron Nitride–Carbon Heteronanotube Junctions, *J. Phys. Chem. Lett.*, 2023, **14**(8), 2056–2064.
40 K. Suenaga, *et al.*, Synthesis of nanoparticles and nanotubes with well-separated layers of boron nitride and carbon, *Science*, 1997, **278**(5338), 653–655.
41 E. Iyyamperumal, S. Wang and L. Dai, Vertically aligned BCN nanotubes with high capacitance, *ACS Nano*, 2012, **6**(6), 5259–5265.
42 W. L. Wang, X. D. B. K. H. Liu, Z. Xu, D. Golberg, Y. Bando and E. G. Wang, Direct Synthesis of B−C−N Single-Walled Nanotubes by Bias-Assisted Hot Filament Chemical Vapor Deposition, *J. Am. Chem. Soc.*, 2006, **128**(20), 6530–6531.
43 O. S. Shaïma Enouz, J.-L. Cochon, C. Colliex and A. Loiseau, C−BN Patterned Single-Walled Nanotubes Synthesized by Laser Vaporization, *Nano Lett.*, 2007, **7**(7), 1856–1862.
44 M.-S. W. Xianlong Wei, Y. Bando and D. Golberg, Electron-Beam-Induced Substitutional Carbon Doping of Boron Nitride Nanosheets, Nanoribbons, and Nanotubes, *ACS Nano*, 2011, **5**(4), 2916–2922.
45 Y. K. Yap, *Hetero-junctions of boron nitride and carbon nanotubes: Synthesis and characterization*, 2013.
46 Z. Liu, *et al.*, In-plane heterostructures of graphene and hexagonal boron nitride with controlled domain sizes, *Nat. Nanotechnol.*, 2013, **8**(2), 119–124.
47 L. Algharagholy, *et al.*, Sculpting molecular structures from bilayer graphene and other materials, *Phys. Rev. B: Condens. Matter Mater. Phys.*, 2012, **86**(7), 075427.
48 X. Blase, *et al.*, Theory of composite B x C y N z nanotube heterojunctions, *Appl. Phys. Lett.*, 1997, **70**(2), 197–199.
49 R. B. Payod and V. A. Saroka, Ab initio study of absorption resonance correlations between nanotubes and nanoribbons of graphene and hexagonal boron nitride, *Semiconductors*, 2019, **53**, 1929–1934.
50 L. Algharagholy, *et al.*, Electronic properties of sculpturenes, *New J. Phys.*, 2014, **16**(1), 013060.
51 S. Tsang, *et al.*, A simple chemical method of opening and filling carbon nanotubes, *Nature*, 1994, **372**(6502), 159–162.
52 D. Hornbaker, *et al.*, Mapping the one-dimensional electronic states of nanotube peapod structures, *Science*, 2002, **295**(5556), 828–831.
53 J. Lee, *et al.*, Bandgap modulation of carbon nanotubes by encapsulated metallofullerenes, *Nature*, 2002, **415**(6875), 1005–1008.
54 T. Takenobu, *et al.*, Stable and controlled amphoteric doping by encapsulation of organic molecules inside carbon nanotubes, *Nat. Mater.*, 2003, **2**(10), 683–688.
55 J. Lu, *et al.*, Amphoteric and controllable doping of carbon nanotubes by encapsulation of organic and organometallic molecules, *Phys. Rev. Lett.*, 2004, **93**(11), 116804.
56 Y. J. Dappe, Encapsulation of organic molecules in carbon nanotubes: role of the van der Waals interactions, *J. Phys. D: Appl. Phys.*, 2014, **47**(8), 083001.
57 K. Mackay, M. Taylor and N. Bajaj, The adverse consequences of mephedrone use: a case series, *Psychiatrist*, 2011, **35**(6), 203–205.
58 P. Grochecki, *et al.*, Effects of mephedrone and amphetamine exposure during adolescence on spatial memory in adulthood: Behavioral and neurochemical analysis, *Int. J. Mol. Sci.*, 2021, **22**(2), 589.
59 E. Olesti, *et al.*, Metabolomics predicts the pharmacological profile of new psychoactive substances, *J. Psychopharmacol.*, 2019, **33**(3), 347–354.
60 S. Duan, *et al.*, Long-term exposure to ephedrine leads to neurotoxicity and neurobehavioral disorders accompanied by up-regulation of CRF in prefrontal cortex and hippocampus in rhesus macaques, *Behav. Brain Res.*, 2020, **393**, 112796.
61 M. Ouyang, *et al.*, *Energy gaps in "metallic" single-walled carbon nanotubes*, *Science*, 2001, **292**(5517), 702–705.
62 C. Zhou, J. Kong and H. Dai, Intrinsic electrical properties of individual single-walled carbon nanotubes with small band gaps, *Phys. Rev. Lett.*, 2000, **84**(24), 5604.
63 R. Hartmann, V. Saroka and M. Portnoi, Interband transitions in narrow-gap carbon nanotubes and graphene nanoribbons, *J. Appl. Phys.*, 2019, **125**(15).
64 G. Fuentes, *et al.*, Formation and electronic properties of BC 3 single-wall nanotubes upon boron substitution of carbon nanotubes, *Phys. Rev. B: Condens. Matter Mater. Phys.*, 2004, **69**(24), 245403.

65 A. Muhulet, *et al.*, Fundamentals and scopes of doped carbon nanotubes towards energy and biosensing applications, *Mater. Today Energy*, 2018, **9**, 154–186.
66 J. Gryko, *et al.*, Low-density framework form of crystalline silicon with a wide optical band gap, *Phys. Rev. B: Condens. Matter Mater. Phys.*, 2000, **62**(12), R7707.
67 R. Romero, *et al.*, Electrical properties of the n-ZnO/c-Si heterojunction prepared by chemical spray pyrolysis, *Mater. Sci. Eng., B*, 2004, **110**(1), 87–93.
68 M. Houssa, *et al.*, First-principles study of the structural and electronic properties of (100) Ge/Ge (M) O 2 interfaces (M= Al, La, or Hf), *Appl. Phys. Lett.*, 2008, **92**(24), 242101.
69 M. Houssa, *et al.*, Electronic properties of two-dimensional hexagonal germanium, *Appl. Phys. Lett.*, 2010, **96**(8), 082111.
70 M. L. Senent and S. Wilson, Intramolecular basis set superposition errors, *Int. J. Quantum Chem.*, 2001, **82**(6), 282–292.
71 M. C. Daza, *et al.*, *Basis set superposition error-counterpoise corrected potential energy surfaces. Application to hydrogen peroxide⋯X (X= F−, Cl−, Br−, Li +, Na +) complexes.* The, *J. Chem. Phys.*, 1999, **110**(24), 11806–11813.
72 W. He, *et al.*, A first principles study on organic molecule encapsulated boron nitride nanotubes, *J. Chem. Phys.*, 2008, **128**(16), 164701.
73 L.-J. Li, *et al.*, Diameter-selective encapsulation of metallocenes in single-walled carbon nanotubes, *Nat. Mater.*, 2005, **4**(6), 481–485.
74 S. Manzetti, Molecular and crystal assembly inside the carbon nanotube: encapsulation and manufacturing approaches, *Adv. Manuf.*, 2013, **1**(3), 198–210.
75 M. Hart, *et al.*, Encapsulation and polymerization of white phosphorus inside single-wall carbon nanotubes, *Angew. Chem.*, 2017, **129**(28), 8256–8260.
76 S. Gorantla, *et al.*, In situ observations of fullerene fusion and ejection in carbon nanotubes, *Nanoscale*, 2010, **2**(10), 2077–2079.
77 J. Sloan, *et al.*, The size distribution, imaging and obstructing properties of C60 and higher fullerenes formed within arc-grown single walled carbon nanotubes, *Chem. Phys. Lett.*, 2000, **316**(3–4), 191–198.
78 B. W. Smith, M. Monthioux and D. E. Luzzi, Encapsulated C60 in carbon nanotubes, *Nature*, 1998, **396**(6709), 323–324.
79 J. Misewich, *et al.*, Electrically induced optical emission from a carbon nanotube FET, *Science*, 2003, **300**(5620), 783–786.
80 G. A. Rance, *et al.*, UV–vis absorption spectroscopy of carbon nanotubes: Relationship between the π-electron plasmon and nanotube diameter, *Chem. Phys. Lett.*, 2010, **493**(1–3), 19–23.
81 M. Arhangelskis, *et al.*, Time-dependent density-functional theory for modeling solid-state fluorescence emission of organic multicomponent crystals, *J. Phys. Chem. A*, 2018, **122**(37), 7514–7521.
82 H. Sadeghi, Discriminating Seebeck sensing of molecules, *Phys. Chem. Chem. Phys.*, 2019, **21**(5), 2378–2381.
83 H. Sadeghi, Quantum and phonon interference-enhanced molecular-scale thermoelectricity, *J. Phys. Chem. C*, 2019, **123**(20), 12556–12562.
84 S. Sirichantaropass, V. García-Suárez and C. J. Lambert, Electronic properties of alkali-and alkaline-earth-intercalated silicon nanowires, *Phys. Rev. B: Condens. Matter Mater. Phys.*, 2007, **75**(7), 075328.
85 J. M. Soler, *et al.*, The SIESTA method for ab initio order-N materials simulation, *J. Phys.: Condens. Matter*, 2002, **14**(11), 2745.
86 D. M. Ceperley and B. J. Alder, Ground state of the electron gas by a stochastic method, *Phys. Rev. Lett.*, 1980, **45**(7), 566.
87 J. P. Perdew, K. Burke and M. Ernzerhof, Generalized gradient approximation made simple, *Phys. Rev. Lett.*, 1996, **77**(18), 3865.
88 G. Abadir, K. Walus and D. Pulfrey, Basis-set choice for DFT/NEGF simulations of carbon nanotubes, *J. Comput. Electron.*, 2009, **8**, 1–9.

